Shallow Water Propagation Incorporating Both Bubble Plumes and Sea-Surface Roughness

Guy V. Norton

Naval Research Laboratory - Stennis Space Center
Stennis Space Center, MS 39529-5004
Email: norton@vixen.nrlssc.navy.mil

Jorge C. Novarini

Planning Systems Incorporated
21294 Johnson Rd. Long Beach, MS 39560-9702
Email: nova@felix.nrlssc.navy.mil

Abstract

The effect of including a range dependent bubble layer and a suitable sea surface spectrum in modeling shallow water propagation is analyzed. Propagation is simulated through a highly accurate model based on a modified PE algorithm which handles surface roughness via conformal mapping. The bubble layer is modeled as a collage of bubble plumes and is included through a complex index of refraction. Propagation at 5 kHz in a 30 m isovelocity waveguide is analyzed in detail.

1. Introduction

Among the many factors affecting the propagation of sound in shallow water, the presence of surface-generated microbubbles has received little attention. The collection of microbubbles which is normally assumed to form a uniform layer, actually presents a very complex structure that varies not only in depth but also in range, and can be characterized as a collage of bubble clouds. This collage creates a strong range-dependent perturbation in the index of refraction and introduces additional attenuation. A numerical procedure is adopted in which a type of bubble cloud (the plume) is modeled following a classification scheme proposed by Monahan [1,2]. The resulting complex index of refraction is then calculated. Since in waveguide propagation the surface roughness mainly causes a re-distribution of energy, the use of a high fidelity model to handle roughness in the presence of strong gradients is essential to obtaining accurate results. An acoustic propagation model, which couples a conformal mapping algorithm to a PE model which properly handles sea surface roughness is used to generate the numerical results [3]. To properly model the sea-surface roughness characteristic of shallow waters, the parametric spectrum GONO has been implemented [4]. The combined effect that the sea surface roughness along with the refractive and lossy bubbly environment have on transmission loss and coherence is examined. The case of a point source, operating at 5 kHz in a 30 m depth isovelociy shallow water waveguide is analyzed in detail.

2. Methodology

2.1 Modeling the Bubble Assemblages

The presence of microbubbles is included through a range-dependent bubble layer made up of different bubble assemblages, namely, bubble plumes and a weak background layer. Due to the lack of information on bubble plumes in shallow water we have adopted and modified a scheme proposed by Monahan for classifying plumes in deep water. Monahan [1,2] postulated the existence of three types of plumes (α, β, γ). He associated two of

them with two stages of whitecap development (stage A and stage B). The α-plume is the subsurface extension of the stage A whitecap which is attached to the crest of the spilling breaker. Although they present the highest void fraction, O (10^{-1} to 10^{-2}), they are very small in size and have a very short lifetime (< 1 sec.). The α-plume quickly decays into a β-plume once the momentum of the downward moving jet associated with the breaking wave is dissipated. Accordingly, the stage A whitecap evolves into a foam patch (stage B whitecap). The β-plumes have a much smaller void fraction, O (10^{-3} to 10^{-4}), and are attached to the foam patch. That is, the stage B whitecap is the top of the β-plume. They are spatially much bigger than the α-plume and have longer lifetimes (about 4 sec). The β-plume then evolves into a γ-plume and eventually detaches from the originating whitecap. The γ-plumes have an even smaller void fraction, O (10^{-6} to 10^{-7}), much larger dimensions, and longer lifetimes (10 to 100 times longer) than the β-plume. They drift and may be affected by circulation processes (such as Langmuir cells). Although Monahan identifies the γ-plume with Thorpe's clouds [5], which allows for both billowy and columnar types, his description of the geometrical aspect (exponentially decreasing cross-section) better fits the columnar type. The γ-plume decays into a weak, stratified background layer with a void fraction, O (10^{-8}). Both the β and γ-plumes are modeled as conical intrusions with cross-sections that decrease exponentially with depth, as prescribed by Monahan and consistent with the v-shape described by Crawford and Farmer [6]. Monahan also provided typical values (void fraction, bubble density at 100 μm, size, penetration scale) for the different bubble assemblages.

In the original Monahan's scheme, the spectral shape for the different stages are essentially identical to each other (spectral slope for large bubbles close to -4). However the bubble concentration and hence the void fraction is different for each plume. However, short time sampling of bubble data gathered close to the surface under breaking waves [7,8,9] show spectral slopes for large bubbles shallower (about -2.5) than those coming from long term averages at deeper depths (-4 and steeper) [10]. Wu suggested that both types of slopes can coexist, the shallower slope close to the breaker and the steeper slope away from the breaker [11]. This can be re-interpreted in terms of Monahan's classification as inside a β-plume for the steeper slope or inside either the γ-plume or the background layer for the shallower slope. Therefore, we have adopted the scheme proposed by Monahan as the basic framework for classifying the different assemblages of microbubbles, with the spectra proposed by Monahan for the different stages having been modified based on more recent findings and Wu's interpretation relating measured spectral slopes for large bubbles with the proximity of the bubble assemblage to the breaker. The α-plumes are not included in the modeling, because of their small size and physical connection to the breaking crests, which are not modeled in the numerical surfaces (the α-plume can be thought of being contained within the crest of the breaking wave).

To parameterize the plumes we have adopted a parameterization scheme similar to that commonly used for the "average, uniform bubble layer," i.e., writing the bubble density per unit volume (bubbles per cubic meter in a 1 μm radius increment) within a given assemblage as

$$n(a,z,u) = N_0\, G(a,z)\, Z(z)\, U(u) \qquad (1)$$

where a is the bubble radius, z is depth, and u is the wind speed. The function G describes the spectral shape, Z the depth dependence, U controls the wind dependence, and N_0 is a constant with controls the bubble density so as to fit Monahan's reference points for the different assemblages (plumes and background layer). Following Monahan, the β-plumes are assumed to have uniform density in depth, while the γ-plume and the background layer decay exponentially. Since, in the present scheme the maximum penetration of the β-plume is assumed to be equal to one-half the significant waveheigth (h_s) of the surface roughness, it is adjusted to the shallow water case by adopting h_s coming from the GONO spectrum which is described in the next section. The cross sectional area of the β and γ-plumes are also exponential in depth. For a full description of the adopted spectra, see Novarini, *et. al.* [12]. Figure 1a shows the bubble density spectra for a 15 m/s wind speed, at 0.25 m below the surface. The collection of plumes are randomized by imposing stochastic fluctuations to: the separation between plumes, the e-folding depth, the area cross-section and the constant N_0 within each realization of the environment.

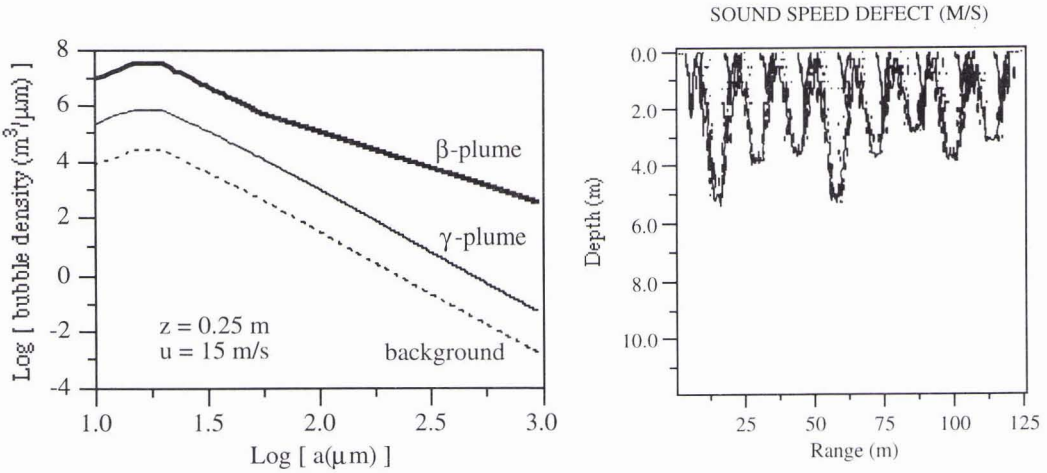

Figure 1 Bubble plume spectra and sound speed defect. a) Bubble spectra for the β and γ-plume, along with the background bubble layer. b) Sound speed defect in m/s, verse depth and range for a 15 m/s wind speed. Contours are 1000 m/s and 1 m/s.

The sound speed perturbation and the additional attenuation are calculated from the change of compressibility introduced by the bubbles. The calculation is carried out following Clay and Medwin [13], integrating over all bubbles, with due regard to viscous and thermal effects. The limits of numerical integration over the bubble radii are 10 and 1000 μm. The effect of the bubbles at a frequency of 5 kHz is to reduce the sound speed and introduce an additional attenuation. Close to the surface (0.25m), for a wind speed of 15 m/s a sound speed defect on the order of 1,210 m/s occurs within the β-plumes (void fraction $8x10^{-4}$). For the γ-plumes the corresponding defect is on the order of 22 m/s (void fraction $1.5x10^{-6}$), while the background layer reduction is about 0.7 m/s (void fraction $5x10^{-8}$). The corresponding attenuation values are 4.4, $6.3x10^{-3}$, and $2x10^{-4}$ dB/cm, respectively. Figure 1b shows a contour plot of the resulting sound speed defect over a short segment of the environment, for a 15 m/s wind. The smaller and sharper intrusions are the 1000 m/s sound speed defect contour which outlines the shape of the β-plumes. The other contour line corresponds to 1 m/s sound speed defect, which essentially delimits the region of significant influence of the γ-plumes. For this example the sound speed defect within the γ-plumes ranges from about 26 m/s very close to the surface to about 0.1 m/s 13m below the surface.

2.2 Modeling the Sea Surface

GONO [4] is a parametric spectrum for wind-driven seas in shallow water. The main parameter is the stage of development ζ of the depth-limited wave growth, defined as

$$\zeta = \sqrt{\frac{h_s}{h_s^{dw}}} \tag{2}$$

where h_s is the significant waveheight for the shallow water site and h_s^{dw} is the corresponding value for a fully developed deep water case at the same wind speed. The spectrum has the form,

$$S(f) = \begin{cases} 0 & 0 \le f \le f_{min} \\ \dfrac{\hat{\alpha} g^2 (f - f_{min})}{(2\pi)^4 f_p^5 (f_p - f_{min})} & f_{min} < f \le f_p \\ \dfrac{\hat{\alpha} g^2}{(2\pi)^4 f^5} & f > f_p \end{cases}$$

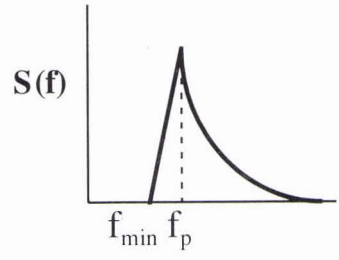

Figure 2. Numerical and graphical representation of the GONO spectrum.

where the spectral parameters are given by the following empirical equations:

$$\hat{\alpha} = \text{modified Phillips "constant"} = 4.93\text{x}10^{-3}\ \zeta^{-1.944} \tag{3}$$

$$\nu = \text{normalized peak freq} = uf_p/g = 6.89\text{x}10^{-2}\ \zeta^{-1.376}/\beta \tag{4}$$

and

$$f_{min} = \mu f_p;\ \mu = \tfrac{1}{2}\left[3 - \frac{4(2\pi)^4 f_p^4 E}{\hat{\alpha} g^2}\right];\ E = \frac{h_s^2}{16};\ \beta = 0.21 \tag{5}$$

The basic assumptions are that dissipation at the bottom is limited to the forward face of the spectrum, and that during the building-up of a wind-driven sea, the bottom dissipation manifests itself rather sharply. The high frequency side of the spectrum has the same decay that the Pierson-Moskowitz spectrum has for deep water (i.e., proportional to f^{-5}). The spectrum requires the knowledge of the significant waveheight for the shallow water site, which can be obtained from satellite observation; visual estimation, etc.. For practical applications in acoustics it is desirable to have the wind speed as the main parameter. A procedure to accomplish this has been developed by Sanders and Bruinsma [4]. It starts with the total energy in the wave system of a deep water case for the given wind speed and assumes all dissipation of the long wave components is due to friction at the bottom. The energy of the wave system is then obtained at the specified water depth by solving an ordinary differential equation with a term describing non-linear dissipation. Once the total energy (E) for the shallow water case is known, the corresponding significant waveheight is given by $h_s = 4\ E^{1/2}$. This value is then used to obtain the spectral shape as outlined above.

Surface realizations of the sea surface (1D) were generated by linear filtering of an array of uncorrelated random numbers whose transfer function is proportional to the square root of the desired power density spectrum. Both GONO and Pierson-Moskowitz spectra are non-directional, originally expressed in terms of the frequency of the waves. They were converted to the wavenumber domain via the dispersion relation connecting frequency with wavenumber for 1-D surfaces, which implicitly assumes all the energy goes in the windward direction.

2.3 Inclusion of Rough Surface

When the effect of the surface roughness is included, it is normally done so by introducing an additional loss mechanism. However, since the surface roughness causes a redistribution of energy, the method of including a loss mechanism to account for the rough surface will not be adequate. Hybrid approaches have been developed to account for the re-distribution of energy induced by the surface roughness. They utilize statistical kernels from sea surface scattering theories in connection with deterministic propagation models [14,15]. Although this type of methodology may improve the calculation of transmission loss, coherence effects are not properly included. Operating in coastal areas where the wave amplitude may become a significant fraction of the water column, strong mode coupling results and perturbative approaches are no longer appropriate. Note that inclusion of a rough surface transforms a range independent problem into a range dependent one.

The approach used to generate the numerical results in this work combines an acoustic propagation model with a conformal mapping algorithm to handle surface roughness in a mathematically consistent manner. The model EFEPE-CM [3] combines the energy-conserving finite element PE propagation model [16] with Dozier's conformal mapping formalism [17] to obtain the acoustic field from a single realization of the environment. The quantities of interest (transmission loss, modal amplitudes, etc.) are then calculated through ensemble averages. The model has been shown to achieve results of benchmark quality for the problem of scattering from randomly rough surfaces [3].

3. Numerical Experiment

The environment for this numerical experiment, is as follows. The water depth is 30 m and constant over a range of 3000 m. An isovelocity, homogeneous water mass was assumed for the bubble-free environment (sound speed = 1500 m/s). The sediment was modeled as a semi-infinite half space of constant sound speed (1541 m/s) and density (1.5 gm/cm^3). Both GONO and Pierson-Moskowitz sea-surface spectra were used to generate the necessary deterministic surfaces. The different surfaces and bubble fields were each characterize by varying the local wind speed (15 and 20 m/s). The acoustic frequency is 5 kHz. The source depth is 5 m.

It is instructive to observe the effect that combining a single β and γ-plume with the background bubble layer has on the propagating field. It is insightful, because we see that even though the individual plumes are small

and spatially do not account for a large area, the effect that they have on the acoustic field is significant. Therefore, utilizing a wind speed of 15 m/s and keeping the sea-surface flat, a single β-plume was placed at a range of 500 m, followed by a γ-plume at a range of 550 m. The β and γ-plume had a width at the surface of approximately 4.5 and 13.5 m respectively. For this example, the plumes did not overlap. The weak background bubble layer spanned the range of 500 to 600 m. The complex acoustic field was determined for this environment. This bubble field was then removed and the complex acoustic field once again determined. The two fields were differenced and the resulting field was converted into an intensity and expressed in dB. Figure 3a depicts this result. Note that before 500 m there is no difference between the two fields since the environments were the same up to this range. However, this rather simple and small bubble field results in multiple beams, one being quite significant. The refractive effects of the two types of bubble plumes can be seen. The process is repeated, except now where the bubbles are present, a rough surface is included (between the ranges of 500 and 600 m). Figure 3b depicts this result. The effect of the rough surface is to redirect the acoustic field at all angles in the forward direction. The beams which were present when the surface is flat have been destroyed. Also note that the strength of the difference for this case (bubble plumes with rough surface and isovelocity with flat surface) is greater than that observed for the previous case.

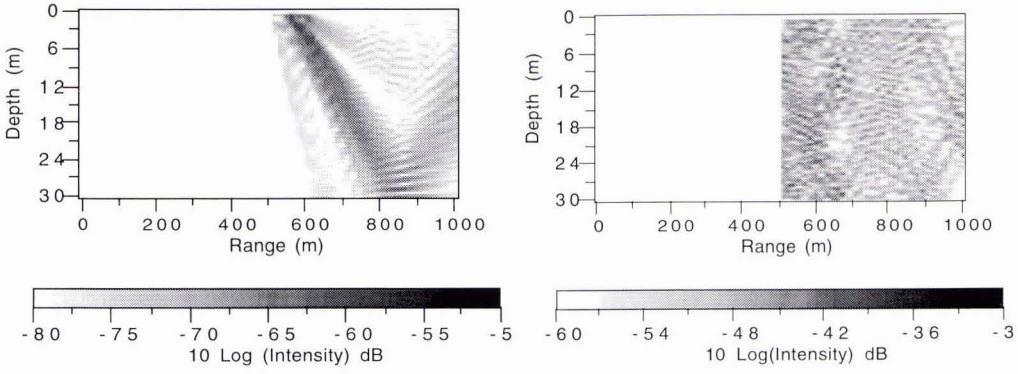

Figure 3. Depth vs. range difference plots. a) Difference in the acoustic fields when a single β, γ-plume and background bubble layer are located between 500 and 600 m and when they are removed. Flat surface used in each case. A wind speed of 15 m/s is assumed. b) Difference in the acoustic fields when a single β, γ-plume and background bubble layer and a rough surface are located between 500 and 600 m and when they are removed. A wind speed of 15 m/s is assumed.

The remaining comparisons will be between environments consisting of rough surfaces using the GONO spectrum with bubble plumes and background bubble layer (bubbles) and rough surfaces using the Pierson-Moskowitz spectrum in the bubble free environment (no bubbles). Two local wind speeds were used, 15 and 20 m/s. These combinations were selected because for the most part bubbles are ignored and when the effect of a rough sea-surface is included, it is often based on a deep water spectrum.

Transmission loss vs. range is now compared for both environments at the two different wind speeds for a single realization of each rough surface. The receiver depth is 15 m, or mid-waveguide depth. Figure 4 depicts the results. Figure 4a compares the results for a wind speed of 15 m/s. Note the GONO with bubbles result (solid line) shows more loss than the Pierson-Moskowitz without bubbles result (dashed line), even though the rms surface height based on the GONO spectrum (1.0 m) is smaller than that from the Pierson-Moskowitz spectrum (1.4 m). This difference in transmission loss is due in large part to the additional attenuation that the plumes introduce. The difference can be as large as 10 dB. Figure 4b is the same comparison except for a wind speed of 20 m/s. Again note that the GONO with bubbles result (solid line) shows more loss than the Pierson-Moskowitz without bubbles result (dashed line), even though the rms surface height based on the GONO spectrum (1.2 m) is smaller than that from the Pierson-Moskowitz spectrum (2.5 m).

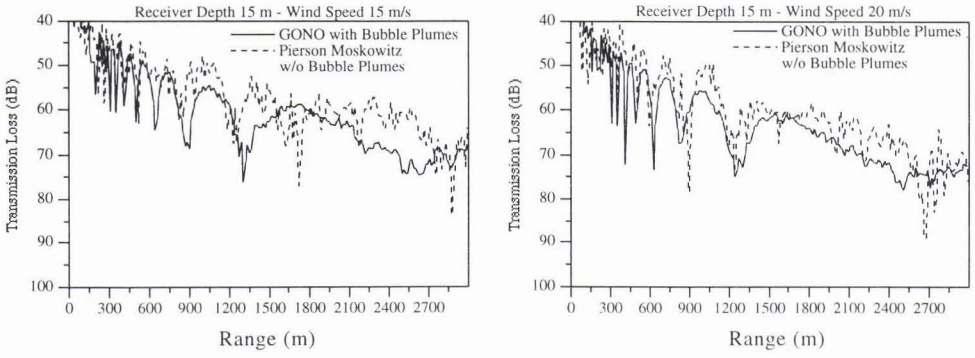

Figure 4. Transmission loss vs. range. a) Receiver depth 15 m, wind speed 15 m/s. GONO with bubbles (solid line) and Pierson-Moskowitz without bubbles (dashed line). b) Receiver depth 15 m, wind speed 20 m/s. GONO with bubbles (solid line) and Pierson-Moskowitz without bubbles (dashed line).

The dependence of transmission loss vs. depth will now be examined using an ensemble of surfaces. Figure 5a shows the results for an ensemble of ten surfaces each from the GONO and Pierson-Moskowitz spectrum. The bubble plumes were used only with the GONO surfaces. The quantity <PP*>, which is proportional to the total intensity, is plotted vs. depth at a range of 3 km. The GONO with bubbles result is the solid line while the Pierson-Moskowitz without bubbles is the dashed line. Note that the result based on the GONO spectrum with bubbles shows more loss throughout the depth of the waveguide and has a maximum difference at the surface. The large difference at the surface is due to the additional attenuation introduced by the bubbles. Overall the two results have the same general shape, showing a notch at approximately 12 m. In addition the Pierson-Moskowitz result has more oscillations in depth. It is of interest to compare the results coming from the present model with those obtained from a standard propagation code under the assumption of a range independent, isovelocity environment (i.e. ignoring bubble plumes and including the rough surface in an approximate manner). To that end we ran SNAP [18], assuming isovelocity water sound speed and with the surface roughness routine activated. The rms surface heights corresponding to the two different spectra for a wind speed of 20 m/s were used. The results are shown in Fig. 5b. The result using 1.2 m rms surface height, corresponding to the GONO surface, is shown with the solid line. The result using 2.5 m rms surface height, corresponding to the Pierson-Moskowitz surface, is shown with the dashed line. The result using the smaller rms surface height shows less loss than when using the larger rms surface height, opposite to what was observed when using EFEPE-CM with an ensemble of rough surfaces. The location of the notch is at 15 m as opposed to 12 m for the EFEPE-CM result.

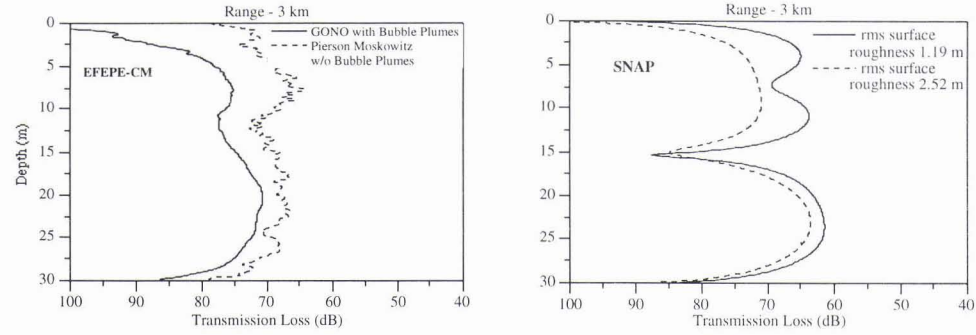

Figure 5. Total field vs. depth. a) Transmission loss vs. depth using EFEPE-CM. Solid line GONO spectrum with bubbles, dashed line Pierson-Moskowitz without bubbles. Ten surfaces in the ensemble. b) Transmission loss vs. depth using SNAP. Solid line, rms surface height 1.19 m (corresponding to GONO spectrum). Dashed line, rms surface height 2.52 m (corresponding to Pierson-Moskowitz spectrum).

Finally the degree of coherence is compared for the two environments (GONO with bubbles and Pierson-Moskowitz without bubbles) at three ranges 1, 2, and 3 km. The degree of coherence is determined by

$$\Gamma = \frac{\left| < PP_0^* > \right|}{\left[< PP^* >< P_0 P_0^* > \right]^{1/2}} \tag{6}$$

where P and P_0 are the complex acoustic pressures for the environment with bubbles and rough surface, and no bubbles and flat surface respectively, while the asterisk (*) denotes the complex conjugate of the corresponding complex acoustic pressure.

Figure 6 depicts the results for the three ranges. Note in each case, the GONO spectrum with bubbles result shows a higher degree of coherence. In addition, the variability in depth decreases with range for both cases but more for the case of the GONO spectrum with bubbles. It is interesting that for both cases the degree of coherence at 1 km has the largest variation which indicates that these fields are most different from the flat surface, isovelocity case at short ranges. This is due to the fact that, initially as the field propagates, the steeper angle (higher-order) modes are stripped-off leaving the interaction with the surface to shallower angle (lower-order) modes. Therefore, the perturbative effect of the surface roughness on the phase of the propagating field diminishes with range. For the case of the GONO spectrum with bubbles, a uniform distribution of Γ with depth is quickly achieved. This is because the high attenuation induced by the bubbles close to the surface prevents the scrambling effect that the rough surface causes on the phase of the propagating field.

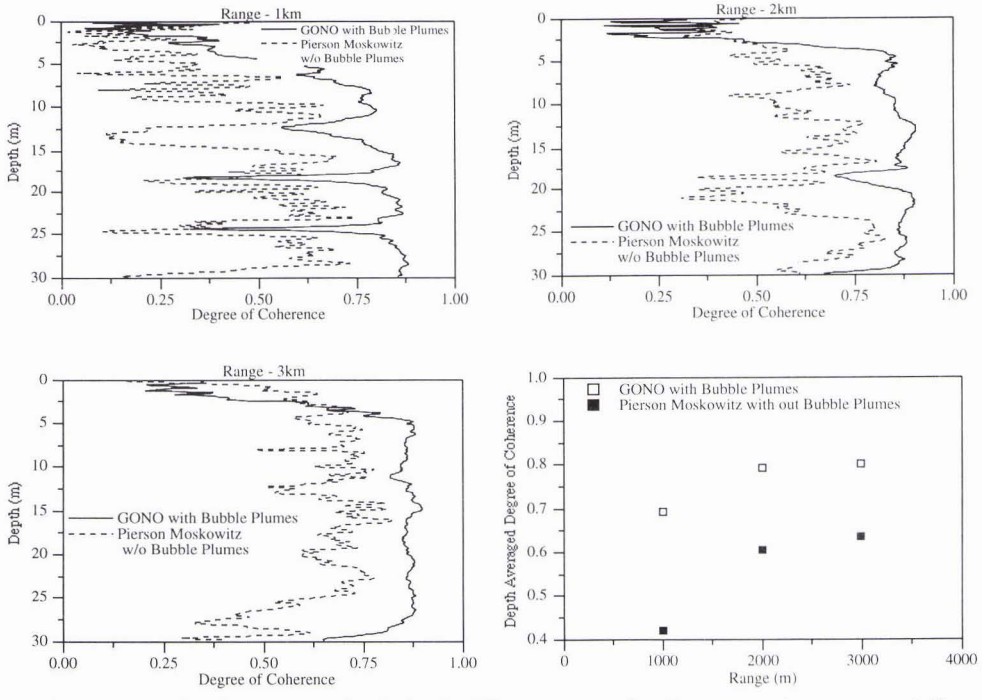

Figure 6. Degree of coherence vs. depth for 3 different ranges for the two environments. a) Degree of coherence vs. depth at 1 km. GONO with bubbles, solid line. Pierson-Moskowitz without bubbles, dashed line. b) Degree of coherence vs. depth at 2 km. GONO with bubbles, solid line. Pierson-Moskowitz without bubbles, dashed line. c) Degree of coherence vs. depth at 3 km. GONO with bubbles, solid line. Pierson-Moskowitz without bubbles, dashed line. d) The depth averaged degree of coherence vs. range for the two environments. GONO with bubbles un-shaded square, Pierson-Moskowitz without bubbles shaded square.

Finally, a depth averaged degree of coherence is obtained by averaging the values obtained at each range over depth. The results are shown in Fig. 6d. At each range, values for the GONO with bubble result are larger than those for the Pierson-Moskowitz without bubbles result. However the trend is the same for each case, that is, the average degree of coherence increases with range. With the limited data shown, it appears that for each case, the average degree of coherence is converging to a different value for each environment.

4. Concluding Remarks

The standard procedure of ignoring the presence of bubble clouds and resorting to a deep water sea-surface spectrum when modeling shallow water propagation at high frequencies leads to significant errors in both, transmission loss and coherence calculations. For the numerical experiment discussed in this work, transmission losses are underestimated by about 5 to 10 dB, and a lower degree of coherence of the propagating field is predicted. Large discrepancies are observed when results from the present model are compared to an acoustic model which treats the waveguide as range independent, ignores bubbles, adopts a deep water sea-surface spectrum and handles surface roughness in an approximate manner.

5. Acknowledgments

This work has been supported by the Office of Naval Research and a grant of HPC time from the DoD HPC Shared Resource Center, CEWES Cray YMP and NAVO Cray C90.

References

[1] Monahan E. C., Proc. 7th Conference on Ocean-Atmosphere Interaction, Anaheim, CA, Amer. Meter. Soc. 188 (1988).

[2] Monahan, E. C. Natural Physical Sources of Underwater Sound, Ed. by B .v R. Kerman, 503, (1993).

[3] Norton, G. V., Novarini, J. C. and R. S. Keiffer, "Coupling scattering from the sea surface to a one-way marching propagation model via conformal mapping: Validation," J. Acoust. Soc. Am. **97**, 2173-2180, (1995).

[4] Sanders J. W. and J. Bruinsma, in Wave dynamics and radio probing of the ocean surface, pp. 615- 637. Edited by O. M. Phillips and K. Hasselmann, Plenum Press, N. Y. (1986).

[5] Thorpe, S. A., "On the clouds of bubbles formed by breaking waves in deep water and their role in the air-sea gas transfer, " Philos. Trans. R. Soc. London Soc. A **304**, 155-210 (1982).

[6] Crawford G. B. and D. M. Farmer, "On the spatial distribution of ocean bubbles," J. Geophys. Res. **92**, C8, 8231-8243 (1987).

[7] Medwin, H. and N. Breitz, "Ambient and transient bubble spectral densities in quiescent seas and under spilling breakers, " J. Geophys. Res. **94**, 12751-12759 (1989).

[8] Su, M. Y., R. Burge and J. Cartmill, "Measurements of near-surface microbubble density during SWADE," (Unpublished).

[9] S. Baldy, "Bubbles in the close vicinity of breaking waves: Statistical characteristics of their generation and dispersion mechanisms," J. Geophys. Res. **93**, 8239-8248 (1988).

[10]Johnson R. C., and B. D. Cooke, " Bubble population and spectra in coastal waters: a photographic approach," J. Geophys. Res. **84,** 3761-3766 (1979).

[11]Wu, J., "Bubbles in the near-surface Ocean: Their various structures," J. Phys. Oceanog. **24**, 1955-1965 (1994).

[12]Novarini, J. C., R. S. Keiffer and G. V. Norton , "A model for variations in the range and depth dependence of the sound speed and attenuation induced by bubble clouds under wind-driven sea surfaces," (Unpublished).

[13]Clay C. S. and H. Medwin, Acoustical Oceanography, John Wiley, New York , pg. 471 (1977).

[14]Dozier, L. B., J. S. Hanna, and C. R. Pearson , in Ocean Variability and Acoustic Propagation, edited by J. Potter and A. Warn-Varnas (Kluwer Academic, Dordrecht), 265-281, (1991).

[15]Schneider, H. G., "Surface loss, scattering and reverberation with the split-step parabolic wave equation model," J. Acoust. Soc. Am. **93**, 770-781 (1993).

[16]Collins, M. D., "A split-step Pade solution for the parabolic equation method," J. Acoust. Soc. Am. **93**, 1736-1742 (1993).

[17]Dozier, L. B., "PERUSE: A numerical treatment of rough surface scattering for the parabolic wave equation," J. Acoust. Soc. Am. **75**, 1415-14432 (1984).

[18]Jensen, F. B. and M. C. Ferla, "SNAP: The SACLANTCEN Normal-mode Acoustic Propagation model," SACLANTCEN Memorandum SM-121, 15 January 1979.